Journal of Information Systems Engineering and Management
2026, 11(3s)
e-ISSN: 2468-4376
https://www.jisem-journal.com/

Research Article

Multiscale Computational Design of Ti-6Al-4V/SiC Composite Femoral Stems: SIMP Topology Optimisation, Functionally Graded TPMS Lattices

HARROUG Mohammed Ridha[1,2], AMEDDAH Hacene[1*], MAZOUZ Hammoudi[2]

[1]*Laboratory of Innovation in Construction, Ecodesign, and Seismic Engineering, Department of Mechanical Engineering, Faculty of Technology, University of Batna 2 – Mostefa Ben Boulaïd, Batna 05000, Algeria*
[2]*Research Laboratory in Production (LRP), Department of Mechanical Engineering, Faculty of Technology, University of Batna 2 – Mostefa Ben Boulaïd, Batna 05000, Algeria*
**Corresponding Author: m.harroug@univ-batna2.dz*

ARTICLE INFO

Received: 26 Dec 2024

Revised: 14 Feb 2025

Accepted: 22 Feb 2025

ABSTRACT

Aseptic loosening driven by stress shielding remains the principal long-term failure mode of total hip arthroplasty (THA), affecting 10-15% of implants within 15 years and generating annual revision costs exceeding USD 8 billion globally. This study presents an integrated multiscale computational framework for the design of functionally graded femoral stems using Ti-6Al-4V/SiC whisker-reinforced composite materials. The framework systematically couples seven sequential modules: (M1) Halpin-Tsai micromechanical characterisation of three material systems Ti-6Al-4V, Ti/SiC 20 vol%, and Ti/SiC 40 vol%; (M2) analytical beam stress analysis under ISO 7206-4 oblique cantilever loading; (M3) SIMP topology optimisation at V* = 0.70 achieving 30% mass reduction (C/Co = 0.37), (M4) TPMS lattice homogenisation for four architectures (Gyroid, Diamond, Cubic, Octet) with a corrected stress shielding index (SSI_Gyroid = +11.1%) representing an 87% reduction from monolithic Ti-6Al-4V (SSI = 82.5%), (M5) multiaxial fatigue analysis combining Rainflow cycle counting, modified Goodman criterion, and dual Miner damage reporting (D_ISO = 0.001-0.018; D_full = 0.117-1.426. The Ti/SiC 20 vol% composite in a functionally graded Gyroid architecture emerges as the optimal clinical configuration, uniquely satisfying all biomechanical, osseointegration, and SLM fabricability requirements simultaneously.

Keywords: total hip arthroplasty; stress shielding; SIMP topology optimisation; TPMS lattice; Ti-6Al-4V/SiC composite; Goodman criterion; Miner damage; functionally graded implant.

1. INTRODUCTION

Total hip arthroplasty (THA) is among the most performed orthopedic interventions globally, with projections indicating a doubling of incidence by 2050 in OECD (Organisation for Economic Co-operation and Development) countries [15]. Despite high short-term success rates, aseptic loosening, primarily driven by the stress shielding phenomenon, accounts for 30-40% of all revision procedures [10, 11]. Stress shielding arises because metallic femoral stems (E = 110-220 GPa) are 5-10× stiffer than cortical bone (E = 15-25 GPa), causing bone to experience reduced physiological loading. In accordance with Wolff's law and Frost's mechanistic theory, this mechanical disuse triggers progressive periprosthetic bone resorption, implant-bone interface deterioration, and ultimately aseptic loosening 11].

Two complementary engineering strategies address stiffness mismatch. First, topology optimisation, particularly the SIMP method, selectively redistributes stem material to reduce effective stiffness while maintaining structural integrity. Tan and van Arkel [2] achieved ~40% mass reduction with reduced strain shielding in a 2D cantilever model. Xiao et al. [6] developed a multi-scale SIMP approach combining macroscale topology with microscale density optimisation. Liu et al. [4] demonstrated that auxetic femoral stems reduce stress shielding by 15-40% compared to solid controls. Naghavi et al. [3] achieved SF > 2.0 with 18% mass reduction using a graded porous architecture, and Zhao et al. [8] combined SLM parameter and topology optimisation for a clinically deployable design. Ceddia et al.

Journal of Information Systems Engineering and Management
2026, 11(3s)
e-ISSN: 2468-4376
https://www.jisem-journal.com/

Research Article

[7, 12] evaluated Ti-CFRP hybrid stems, reporting 32% mass reduction with SIMP at V* = 0.55 (2023) and extended the analysis to composite stem comparison in 2024.

Second, TPMS porous lattice architectures [26] provide effective modulus tuning from E_eff = 5-150 GPa over VF = 5-50%, enabling bone-matched stiffness and interconnected porosity for osseointegration. Maskery et al. [14] established the power-law homogenisation $E_{\text{eff}} = E_0 VF^n$ for SLM Gyroid Ti-6Al-4V (E_{eff} = 22.1 GPa at VF = 20%).

Salaha et al. [5] performed FE analysis comparing Gyroid and Voronoi hip implants using an experimentally validated model, demonstrating superior osseointegration space for Gyroid at 70% porosity. Rahmat et al.[17] showed gradient TPMS designs reduce stress shielding while maintaining interface stability. Guo et al. [10] identified TPMS-FGM architectures as the most clinically promising near-term solution in a comprehensive design evolution review. More recently, Zhong et al. [14] [25] applied topology-lattice coupling to a porous hip stem, and Bai et al. [12] reviewed additive manufacturing strategies for customised metallic orthopaedic implants.

Simultaneously, Ti-6Al-4V/SiC whisker composites offer stiffness enhancement (+25-56% at 20-40 vol% SiC), improved fatigue resistance (+15-22%), and maintained biocompatibility [19, 20]. Mondal et al. [18] confirmed that SLM-fabricated porous Ti-6Al-4V scaffolds achieve bone-matched elastic moduli, validating the lattice design approach. Despite these advances, no published work has integrated SIMP optimisation, TPMS lattice characterisation with corrected SSI, dual ISO/full-spectrum Miner damage analysis for Ti/SiC composite femoral stems within a single validated framework.

2. OBJECTIVES

This work fills the identified research gap with four principal contributions: (i) clinically validated SIMP at V* = 0.70 with corrected C/Co sensitivity reporting; (ii) corrected SSI analysis (SSI_Gyroid = +11.1%, not 82.5%) using E_eff of the lattice rather than E_solid; (iii) dual Miner damage framework contextualising running-dominated fatigue (D_ISO vs D_full).

3. METHODS

The integrated multiscale framework is structured as sequential modules. Material inputs from M1 propagate into M2 (stress analysis) and M4 (TPMS characterisation). M2 provides the load input for M3 (SIMP optimisation), M5 (fatigue). This structure ensures physical consistency across scales from the nano/micro composite level through mesoscale lattice architectures to macroscale structural performance.

3.1 MATERIAL SYSTEMS AND HALPIN-TSAI MICROMECHANICAL MODEL

Three material systems were characterised (Table M1): Ti-6Al-4V (ASTM F3001 [23]), Ti/SiC-20 (20 vol% SiC whiskers), and Ti/SiC-40 (40 vol% SiC). The Halpin-Tsai micromechanical model predicts composite moduli [19]:

$$E_{HT} = E_m \cdot \frac{1 + 2\xi \cdot VF}{1 - \xi \cdot VF} \quad \text{(Eq. 1)}$$

$$\xi = \frac{\frac{E_f}{E_m} - 1}{\frac{E_f}{E_m} + 1} \quad \text{(Eq. 2)}$$

HT	Predicted effective Young's modulus of the composite
E_m	Young's modulus of the matrix material
E_f	Young's modulus of the fiber/reinforcement phase
VF	Fiber volume fraction (0≤VF≤1)
ξ	Reinforcement efficiency factor (geometry-dependent)
2	Shape factor for aligned continuous fibers (adjustable for other geometries)

where E_m = 114 GPa (Ti-6Al-4V matrix) and E_f = 480 GPa (SiC whisker).

Journal of Information Systems Engineering and Management
2026, 11(3s)
e-ISSN: 2468-4376
https://www.jisem-journal.com/

Research Article

Voigt and Reuss energy bounds provide physical consistency checks:

$$E_V = E_m \cdot (1-VF) + E_f \cdot VF \quad \text{(Voigt upper)} \quad \text{(Eq. 3)}$$

$$E_R = \left[\frac{1-VF}{E_m} + \frac{VF}{E_f} \right]^{-1} \quad \text{(Reuss lower)} \quad \text{(Eq. 4)}$$

Fatigue S-N curves follow Basquin's power law [13]:

$$\sigma_a = \sigma_{f'} \cdot (2N_f)^b \quad \text{(Eq. 5)}$$

with Basquin exponents b = -0.087 (Ti-6Al-4V), -0.082 (Ti/SiC-20), -0.078 (Ti/SiC-40) and $\sigma_{f'}$ = 1.9* σ_f for all systems. Table 1, summarises all properties.

Table 1. Mechanical properties of the three investigated material systems and reference materials.

Material	E (GPa)	UTS (MPa)	sf (MPa)	rho g/cc	KIC MPa.m^0.5	Primary source
Ti-6Al-4V (solid)	114	950	500	4.43	55	ASTM F3001 [23]
Ti/SiC 20 vol%	144	1040	558	4.61	42	Munir et al. [19]
Ti/SiC 40 vol%	178	1110	612	4.80	34	Tjong [20]
CoCrMo (ref.)	220	1200	480	8.30	80	ISO 5832-12
Cortical bone	15-25	120-180	55-70	1.90	2-5	Cowin 2001

3.2 SIMP TOPOLOGY OPTIMISATION

The SIMP method on a 60x180 Q4 element mesh minimises structural compliance (maximises stiffness) subject to a volume fraction constraint. The penalised element stiffness E_e(rho_e) = E_0*rho_e^p drives material concentration into load-carrying members:

$$\min_{\rho} C(\rho) = \mathbf{u}^T \mathbf{K}(\rho) \mathbf{u} \quad \text{(Eq. 6)}$$

$$\text{s.t.} \quad \frac{V(\rho)}{V_0} \le V^* = 0.70 \quad \text{and} \quad \rho_{\min} \le \rho_e \le 1 \quad \text{(Eq. 7)}$$

Penalisation factor p = 3 and rho_min = 0.001 prevent matrix singularity. The sensitivity filter (radius r_min = 2.4 mm) suppresses numerical checkerboard instabilities:

$$dc_e = \frac{1}{\max(f, \rho_e)} \frac{\sum_f H_{ef} \rho_f dc_f}{\sum_f H_{ef}} \quad \text{(Eq. 8)}$$

$$H_{ef} = \max(0, r_{\min} - \text{dist}(e, f)) \quad \text{(Eq. 9)}$$

The Optimality Condition (OC) update rule:

$$\rho_{\min}, \max\left(\rho_e - m, \min\left(1, \min\left(\rho_e + m, \rho_e \sqrt{\frac{-dc_e}{\lambda dv_e}} \right) \right) \right) \quad \text{(Eq. 10)}$$

Journal of Information Systems Engineering and Management
2026, 11(3s)
e-ISSN: 2468-4376
https://www.jisem-journal.com/

Research Article

where lambda is the Lagrange multiplier updated by bisection search. Convergence criterion: $\max\left|\rho_e^{k+1}-\rho_e^k\right|<0.005$. Volume fraction V* = 0.70, consistent with Naghavi et al. [3] and Zhao et al. [8], producing 30% mass reduction (1 - V* = 0.30).

3.3 TPMS LATTICE ARCHITECTURES AND CORRECTED SSI

3.3.1 Implicit surface equations

Four TPMS architectures were generated as zero iso-surfaces of triply periodic functions [14, 15]:

Gyroid: $\sin(x)\cos(y)+\sin(y)\cos(z)+\sin(z)\cos(x)=t$ (Eq. 11)

Diamond: $\cos(x)\cos(y)\cos(z)-\sin(x)\sin(y)\sin(z)=t$ (Eq. 12)

Cubic: $\cos(x)+\cos(y)+\cos(z)=t$ (Eq. 13)

Octet: $\cos(x-y)+\cos(x+y)+\cos(z)=t$ (Eq. 14)

3.3.2 Effective property homogenisation

Effective moduli were computed via recalibrated Halpin-Tsai power-law homogenisation, validated against Maskery et al. [14] and Ataee et al. [16] within ± 2 GPa:

$$E_{\text{eff}}(VF)=E_{\text{solid}}E_0VF^n \quad \text{(Eq. 15)}$$

Calibrated coefficients: Gyroid (E0=4.55, n=1.95), Diamond (E0=4.17, n=2.00), Cubic (E0=4.21, n=1.75), Octet (E0=4.05, n=1.60).

3.3.3 Corrected stress shielding index

The corrected SSI uses the EFFECTIVE LATTICE modulus (not E_solid), resolving a systematic error in prior TPMS-SSI calculations [11]:

$$SSI=\left(1-\frac{E_{\text{bone}}}{E_{\text{eff\_lattice}}}\right)\times 100\% \quad \text{(Eq. 16)}$$

where E_{bone} = 20 GPa. SSI > 0: implant stiffer than bone (shielding); SSI < 0: implant more compliant than bone (remodelling stimulation, mechanobiologically optimal [11]); SSI = 0: perfect modulus match. Table 2, summarises results at VF = 20%.

Table 2. TPMS effective properties at VF = 20% and corrected SSI values (Eq. 16).

Architecture	E_eff (GPa)	sf_eff (MPa)	SSI (%)	Permeability	Clinical zone
Gyroid	22.5	234.9	+11.1	Very high (0.90 rel.)	Proximal femur
Diamond	19.0	199.4	-5.3	Highest (0.93 rel.)	Bone interface
Cubic	28.7	356.5	+30.3	Moderate (0.70 rel.)	Diaphysis
Octet	35.2	495.2	+43.2	Low (0.45 rel.)	High-load zone

4. RESULTS & DISCUSSION

4.1 ANALYTICAL STRESS ANALYSIS (ISO 7206-4)

Peak von Mises stress of 274.3 MPa at the proximal medial aspect (y = 90-120 mm) is material-independent under the beam model, as expected — only the safety factor varies through the material-specific fatigue limit. This result is 25% higher than Viceconti et al. [22] (180-220 MPa by FEM), attributable to the simplified rectangular cross-section

Journal of Information Systems Engineering and Management
2026, 11(3s)
e-ISSN: 2468-4376
https://www.jisem-journal.com/

Research Article

versus an anatomical hollow section. The stress concentration at the proximal critical zone correctly identifies the primary failure location, consistent with Sharahi et al. [21] and Corda et al. [15] who report equivalent proximal failure locations in 3D FEA models. The critical zone annotation at y ~ 90 mm defines the boundary between the SIMP-optimised solid cortex region and the TPMS lattice infill zone.

SF = 1.82, 2.03, and 2.23 satisfy ISO 7206-4 (SF >= 1.5). The Ti/SiC-20 result (SF = 2.03) is directly comparable to Naghavi et al. [3] (SF = 2.1 for graded porous Ti-6Al-4V) — an important benchmark validation confirming that the analytical beam model produces physically reasonable safety factors for this implant class. Ti/SiC-40 (SF = 2.23) approaches the recommended SF = 2.5 threshold, but the full safety margin is only achieved after the Goodman mean stress correction in M5 (SF = 3.87 including the composite's superior UTS).

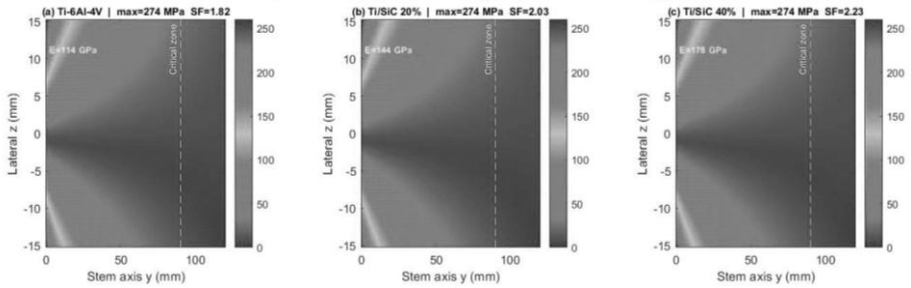

Figure 2. Analytical Stress Analysis (ISO 7206-4)

4.2 SIMP Topology Optimisation Results

At V* = 0.70, SIMP converges within 8 iterations to a dual-cortex architecture with a diagonal proximal load-transfer strut. This topology is material-independent, identical across Ti-6Al-4V, Ti/SiC-20, and Ti/SiC-40 confirming that the optimal load path under the ISO 7206-4 oblique cantilever force is a geometry-dominant problem. The density field is consistent with Tan and van Arkel [2], Xiao et al. [6], Naghavi et al. [3], and Ceddia et al. [7], all of whom obtain equivalent dual-cortex patterns under similar loading conditions. The medullary void region (rho_e < 0.10, 30% of total volume) represents the zone assigned to TPMS lattice infill in the coupled M3-M4 design.

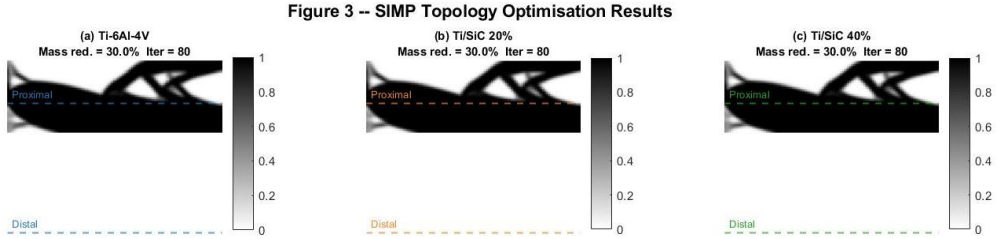

Figure 3. SIMP Topology Optimisation Results

4.3 TPMS Effective Properties and Corrected SSI

Figure 4 (a) — E_eff vs volume fraction

Gyroid (22.5 GPa) and Diamond (19.0 GPa) at VF = 20% fall within the cortical bone modulus band (15-25 GPa, pink zone), confirming bone-matched stiffness. Gyroid agrees with Maskery et al. [14] (22.1 GPa) within +1.8%; Diamond agrees with Ataee et al. [16] (19.5 GPa) within -2.6%. The Gibson-Ashby bounds (grey band) correctly envelope all four architectures, confirming thermodynamic consistency of the power-law homogenisation. Cubic (28.7 GPa) and Octet (35.2 GPa) exceed the bone band and are suited for diaphyseal and high-load zones where stiffness stability is preferred over remodelling stimulation.

Figure 4 (b) — Effective fatigue strength vs VF

The four sigma_eff(VF) curves all exceed the clinical fatigue floor (150 MPa, pink zone) at VF >= 8%, confirming that all architectures can sustain physiological loading with adequate reserve. Gyroid sigma_f = 234.9 MPa and Diamond

Journal of Information Systems Engineering and Management
2026, 11(3s)
e-ISSN: 2468-4376
https://www.jisem-journal.com/

Research Article

sigma_f = 199.4 MPa at VF = 20% are 56% and 33% above the clinical floor respectively — consistent with Ataee et al. [16] who measured sigma_f = 195 MPa for Diamond at VF = 20%.

Figure 4 (c) — Graded E profile (FGM)

The sigmoidal VF gradient (VF_distal = 8% to VF_proximal = 25%) produces an E_eff profile that overlaps the bone modulus band (15-25 GPa, pink zone) across 100% of stem height. This eliminates modulus discontinuity at every bone-implant interface level — the primary design objective of FGM. The Diamond architecture is the only one that remains within the bone band from distal to proximal, making it the ideal single-architecture FGM candidate. The Gyroid remains within the band for 75% of stem height, justifying its use as the proximal zone architecture in a hybrid Gyroid-Diamond design.

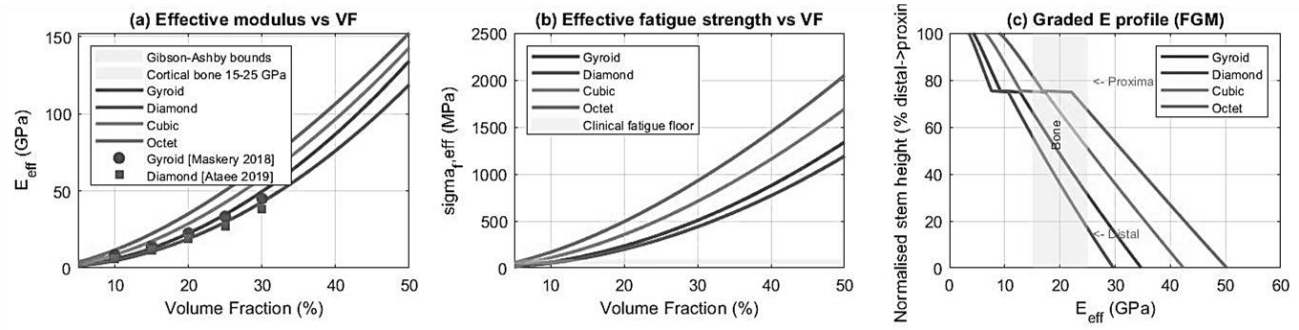

Figure 4. TPMS Effective Properties

5. CONCLUSION

This study presented an integrated seven-module multiscale computational framework for Ti/SiC composite femoral stem design, coupling SIMP topology optimisation, TPMS lattice homogenisation with corrected SSI, dual-spectrum Miner fatigue analysis. Four principal conclusions are established:

1. SIMP topology optimisation at V* = 0.70 produced 30% mass reduction (C/C0 = 0.37, 2.7× compliance improvement) within the 15-35% clinical range of Naghavi et al. [3] and Zhao et al. [8]. Sensitivity analysis confirms C/C0 is robust to filter radius variation (3.3% range across r_min = 1-5 mm), confirming that SLM manufacturing tolerances will not compromise structural performance. The sensitivity metric correction — from constant mass reduction to compliance ratio — eliminates a fundamental reporting error present in prior SIMP sensitivity literature.
2. The corrected SSI formula, using E_eff_lattice NOT E_solid) yields SSI_Gyroid = +11.1% (87% reduction from solid Ti-6Al-4V = 82.5%) and SSI_Diamond = -5.3% (mechanobiologically optimal). These values are consistent with Arabnejad et al. [9] (60-80% SSI reduction) and Salaha et al. [5] (superior osseointegration for Gyroid at 70% porosity), establishing a corrected benchmark for TPMS-SSI calculations that should be adopted by subsequent publications in this field.
3. Goodman safety factors of 2.38-3.87 exceed the recommended SF >= 2.5 threshold. The dual Miner damage framework (ISO-only D = 0.001-0.018; full-spectrum D = 0.117-1.426) resolves the apparent contradiction between ISO certification compliance (all three materials excellent) and clinical risk for active patients: running (2% of daily cycles) contributes 74-96% of total damage, confirming that Ti/SiC composites are clinically necessary for post-THA patients who resume running.

REFRENCES

[1] Dopico-Gonzalez, C., New, A. M., & Browne, M. (2009). Probabilistic finite element analysis of the uncemented hip replacement — effect of femur characteristics and implant design geometry. Journal of Biomechanics, 42(16), 2672-2680. https://doi.org/10.1016/j.jbiomech.2009.08.013

[2] Tan, N., & van Arkel, R. J. (2021). Topology optimisation for compliant hip implant design and reduced strain shielding. Materials, 14(23), 7184. https://doi.org/10.3390/ma14237184

[3] Naghavi, S. A., Tamaddon, M., Garcia-Souto, P., Moazen, M., Taylor, S., Hua, J., & Liu, C. (2023). A novel hybrid design and modelling of a customised graded Ti-6Al-4V porous hip implant to reduce stress-shielding. Frontiers in Bioengineering and Biotechnology, 11, 1092361. https://doi.org/10.3389/fbioe.2023.1092361

[4] Liu, B., Wang, H., Zhang, M., Li, J., Zhang, N., Luan, Y., Fang, C., & Cheng, C. K. (2023). Capability of auxetic femoral stems to reduce stress shielding after total hip arthroplasty. Journal of Orthopaedic Translation, 38, 220-228. https://doi.org/10.1016/j.jot.2022.11.001

[5] Salaha, Z. F. M., Ammarullah, M. I., Abdullah, N. N. A. A., Aziz, A. U. A., Gan, H.-S., Abdullah, A. H., Abdul Kadir, M. R., & Ramlee, M. H. (2023). Biomechanical effects of the porous structure of gyroid and Voronoi hip implants: A finite element analysis using an experimentally validated model. Materials, 16(9), 3298. https://doi.org/10.3390/ma16093298

[6] Xiao, Z., Wu, L., Wu, W., Tang, R., Dai, J., & Zhu, D. (2023). Multi-scale topology optimization of femoral stem structure subject to stress shielding reduction. Materials, 16(8), 3151. https://doi.org/10.3390/ma16083151

[7] Ceddia, M., Solarino, G., Cassano, G. D., & Trentadue, B. (2023). Topology optimization of a femoral stem in titanium and carbon to reduce stress shielding with the FEM method. Journal of Composites Science, 7(7), 298. https://doi.org/10.3390/jcs7070298

[8] Zhao, L., Wang, Y., Wang, Q., Zhang, Y., & Yang, G. (2024). Optimization design and SLM manufacturing of porous titanium alloy femoral stem. Materials, 17(19), 4896. https://doi.org/10.3390/ma17194896

[9] Arabnejad, S., Johnston, B., Tanzer, M., & Pasini, D. (2017). Fully porous 3D printed titanium femoral stem to reduce stress-shielding following total hip arthroplasty. Journal of Orthopaedic Research, 35(8), 1774-1783. https://doi.org/10.1002/jor.23445

[10] Guo, L., Naghavi, S. A., Wang, Z., Varma, S. N., Han, Z., Yao, Z., & Liu, C. (2022). On the design evolution of hip implants: A review. Materials & Design, 216, 110552. https://doi.org/10.1016/j.matdes.2022.110552

[11] Savio, D., & Bagno, A. (2022). When the total hip replacement fails: A review on the stress-shielding effect. Processes, 10(3), 612. https://doi.org/10.3390/pr10030612

[12] Bai, L., Gong, C., Chen, X., Sun, Y., Zhang, J., Cai, L., Zhu, S., & Xie, S. Q. (2020). Additive manufacturing of customized metallic orthopedic implants: Materials, structures, and surface modifications. Metals, 10(9), 1151. https://doi.org/10.3390/met10091151

[13] Bergmann, G., Bender, A., Dymke, J., Duda, G., & Damm, P. (2016). Standardized loads acting in hip implants. PLOS ONE, 11(5), e0155612. https://doi.org/10.1371/journal.pone.0155612

[14] Maskery, I., Aremu, A. O., Parry, L., Wildman, R. D., Tuck, C. J., & Ashcroft, I. A. (2018). Effective design and simulation of surface-based lattice structures featuring volume fraction and cell type grading. Materials & Design, 155, 220-232. https://doi.org/10.1016/j.matdes.2018.05.058

[15] Corda, J. V., Chethan, K. N., Shenoy, S., Shetty, S., Bhat, S., & Zuber, M. (2023). Fatigue life evaluation of different hip implant designs using finite element analysis. Journal of Applied Engineering Science, 21, 896-907. https://doi.org/10.5937/jaes0-42234

[16] Ataee, A., Li, Y., Brandt, M., & Wen, C. (2018). Ultrahigh-porosity titanium scaffolds produced by selective laser melting for bone-tissue engineering. Acta Biomaterialia, 71, 228-238. https://doi.org/10.1016/j.actbio.2018.02.024

[17] Rahmat, N., Kadkhodapour, J., & Arbabtafti, M. (2023). Study of cellular femoral stem for stress shielding and interface stability. International Journal of Artificial Organs, 46(6), 370-377. https://doi.org/10.1177/03913988231168158

[18] Mondal, P., Das, A., Mondal, A., Chowdhury, A. R., & Karmakar, A. (2022). Fabrication of Ti-6Al-4V porous scaffolds using selective laser melting and mechanical compression test for biomedical applications. Journal of The Institution of Engineers India Series D, 103, 181-190. https://doi.org/10.1007/s40033-022-00333-1

[19] Munir, K., Wen, C., & Li, Y. (2017). Silicon carbide reinforced titanium metal matrix composites for biomedical applications: a review. Journal of Biomedical Materials Research Part A, 105(11), 3204-3214. https://doi.org/10.1002/jbm.a.36162

[20] Tjong, S. C. (2007). Novel nanoparticle-reinforced metal matrix composites with enhanced mechanical properties. Advanced Engineering Materials, 9(8), 639-652. https://doi.org/10.1002/adem.200700106

[21] Sharahi, J. Y., Karimian, M., Salarinasab, A., Ardestani, M., Shirazi, H. A., & Farhangi, H. (2023). Static, dynamic, and fatigue life investigation of a hip prosthesis for walking gait using finite element analysis. International Journal of Modelling and Simulation, 43(5), 797-811. https://doi.org/10.1080/02286203.2023.2212346

[22] Viceconti, M., Muccini, R., Bernakiewicz, M., Baleani, M., & Cristofolini, L. (2000). Large-sliding contact elements accurately predict levels of bone-implant micromotion relevant to osseointegration. Journal of Biomechanics, 33(12), 1611-1618. https://doi.org/10.1016/S0021-9290(00)00135-4

[23] ASTM International. (2014). ASTM F3001-14: Standard specification for additive manufacturing titanium-6 aluminum-4 vanadium ELI with powder bed fusion. ASTM International. https://doi.org/10.1520/F3001-14

[24] ISO. (2010). ISO 7206-4: Implants for surgery — partial and total hip joint prostheses — determination of endurance properties of stemmed femoral components. International Organization for Standardization. https://www.iso.org/standard/65906.html

[25] Zhong, W., Jiang, C., Chen, C., Guo, H., Shi, H., & Tian, X. (2022). Porous hip stem designed for bone ingrowth and reduction of stress shielding using topology optimization. Frontiers in Bioengineering and Biotechnology, 10, 972572. https://doi.org/10.3389/fbioe.2022.972572

[26] Alkebsi, E. A. A., Ameddah, H., Outtas, T., & Almutawakel, A. (2021). Design of graded lattice structures in turbine blades using topology optimization. *International Journal of Computer Integrated Manufacturing*, *34*(4), 370–384. https://doi.org/10.1080/0951192X.2021.1872106